 DOI: 10.1002/masy.200950814

Estimating Slow Crack Growth Performance of Polyethylene Resins from Primary Structures such as Molecular Weight and Short Chain Branching

Paul J. DesLauriers, David C. Rohlfing*

Summary: Molecular weight and short chain branching (SCB) data experimentally obtained by SEC-FTIR are combined into a single, primary structural parameter (*PSP2*) and used to rapidly screen the slow crack growth resistance of a variety of polyethylene resins. Our results show that *PSP2* values obtained for resins made using different catalysts (both dual and single catalyst systems) and hence, different polymer architectures, correlate well with results obtained from several short-term tensile tests. The development of *PSP2*, as well as the qualitative and quantitative predictive ability of this parameter are presented and discussed.

Keywords: polyethylene; primary structure parameter; SEC-FTIR; short chain branching; slow crack growth; structure property relations

Introduction

Many small-scale tests (such as tensile testing, PENT, etc.) have been developed over the years to predict the resin's potential to resist slow crack growth (SCG). Although some of these tests (e.g., tensile) are not very time consuming or expensive, other tests, especially for the higher performance resins, can take long periods of time (e.g., >6,000 h in the case of PENT testing) and are ultimately dependent on a mechanical measurement of the sample. If one could estimate the mechanical properties of a pipe resin based solely upon its primary polymer structure, such as the molecular weight (MW) and short chain branching (SCB) distributions, the cycle time for product development could be drastically reduced.

Coupling size exclusion chromatography (SEC) and on-line Fourier transform infrared spectroscopy (FTIR) provides a convenient way to gain both MW data as well as comonomer distribution across the MWD as shown by DesLauriers *et. al.*[1–3] Furthermore, the primary structural information afforded from SEC-FTIR can be empirically correlated to a resin's mechanical properties. For example, recent work by DesLauriers[4] has shown that PENT values for polyethylene resins can be directly correlated to polymer structure by calculating a slice by slice, cross product term involving molecular weight, weight fraction, and SCB level over the whole molecular weight distribution. By plotting this term against log *M* and taking the area underneath the resulting curve, a single quantity defined as the Primary Structure Parameter (*PSP1*) was obtained and correlated to PENT values for several types of polyethylene resins.

Although each type of polyethylene (i.e., based on catalyst type and modality) required separate calibration curves for the observed correlations, a subsequent universal calibration curve was also developed by DesLauriers[4] using chemometric techniques. Of course, this methodology is still an empirical approach, the accuracy and precision of which is dependent on a number of variables (e.g. training set composition, MW calibration curve,

Chevron Phillips Chemical Company LP, Bartlesville, OK 74004, USA
E-mail: deslapj@cpchem.com

detector sensitivity, etc.; also see references 1 and 2).

In this paper we discuss and further elaborate on another primary structural parameter (*PSP2*), also recently developed[4] that is based on a more fundamental approach. This new structural parameter is calculated using densities estimated from experimentally obtained SEC-FTIR data and probability equations for tie molecule formation, as developed by Huang & Brown.[5] Using this approach, *PSP2* values were calculated for a variety of polyethylene resins with different architectures and compared to tensile test results for these same resins.

Experimental Part

All measurements were made on pellets samples of polyethylene homopolymers and 1-hexene copolymers. Density measurements were made using ASTM D1505. All density plaques were made according to ASTM D4703 (Annex A1, Procedure C) and allowed to sit at room temperature for at least 40 h before testing. Molecular weights and molecular weight distributions were obtained using a PL220 SEC high temperature chromatography unit (Polymer Laboratories) with trichlorobenzene (TCB) as the solvent, with a flow rate of 1 mL/minute at a temperature of 145 °C. BHT (2,6-di-tert-butyl-4-methylphenol) at a concentration of 0.5 g/L was used as a stabilizer in the TCB. An injection volume of 200 μL was used with a nominal polymer concentration of 1.5 mg/mL. The columns used were three PLgel Mixed A LS columns (7.8 × 300 mm) and were calibrated with a broad linear polyethylene standard (Phillips Marlex® BHB 5003) for which the molecular weight had been determined using a Dawn EOS multiangle light scattering detector (Wyatt). SCB data were obtained using a SEC-FTIR high temperature heated flow cell (Polymer Laboratories) as previously outlined.[1] Short-term tensile tests were performed using the following standards: Pennsylvania Notch Test (PENT; ASTM F1473), Single Point Notched Constant Tensile Load test (SP-NCTL; ASTM D5397; 30% yield) and Natural Draw Ratio (NDR; ASTM D638), where NDR is the extent at which strain hardening occurs.

Results and Discussion

Density Calculations

The first step in assessing the influence of structure on slow crack growth in polyethylene resins is to evaluate the effects of structure on the reported density for the bulk polymer and to account for these effects on a MW slice-by-slice basis. There are many factors that go into determining the solid density a polyethylene polymer will have. Density is really not a fundamental property of a polymer, although it is often treated as such. It is a combination of structural properties, processing variables, and heating and cooling rates that determine the density of a final part. In these studies, all measured densities are assumed to reflect equilibrium conditions (see Experimental).

Structural properties that affect the density of polyethylene polymers include molecular weight as well as both the amount and distribution of short chain branching (SCB) in the polymer. Both types of primary structures influence the level of crystallinity in the polymer. In order to better quantify the effect of MW on density, the MWD profiles (as determined by SEC) for a set of relatively narrow MWD homopolymers (PDI ~ 3.0), whose crystallinity and crystallizing behavior were originally reported by Jordens *et. al* [6] were re-evaluated (Table 1).

A cursory look at this data suggests that there is a linear relationship between homopolymer density and Log *M*. This relationship also implies that by using the appropriate calibration curve, the homopolymer density of a bulk polymer can be estimated by summing (slice by slice) the specific volumes ($1/\rho_i$) weighted by the weight fractions (w_i) of the various

Table 1.
Selected properties for polyethylene homopolymer samples.

Sample	Nominal M_w (kg/mol)	Nominal M_p (kg/mol)	Nominal PDI	Measured density (g/cm^3)	Calculated density (g/cm^3)*
1	750	701	3.5	0.938	0.940
2	368	312	2.6	0.944	0.945
3	283	196	3.4	0.947	0.950
4	201	138	2.5	0.951	0.952
5	193	174	3.5	0.950	0.954
6	135	96	3.1	0.955	0.957
7	70	50	2.8	0.964	0.963
8	51	42	2.3	0.969	0.966
9	35	24	3.6	0.973	0.972
10	25	20	2.5	0.975	0.974
11	20	10	3.2	0.976	0.977

*See text.

components that make up the MWD profile as given in Equation 1. The coefficients a and b in this equation were determined by a least square fit to the SEC data for those samples reported in Table 1.

$$1/\rho = \sum (w_i/\rho_i) = \int \tfrac{1}{\rho}\left(\tfrac{dw}{dLogM}\right) dLogM \quad (1)$$

where: $\rho = [a - bLogM]$

In this work, the following equation was used to estimate homopolymer density from molecular weight:

$$\rho = 1.0748 - (0.0241) Log\, M. \quad (2)$$

However, we should note that a linear relationship between molecular weight and density will overestimate the density at very low molecular weights and the selection of what density represents the maximum density (i.e., the density of 100% crystalline PE) will dictate how much of the MWD should be used in the calculation. For example, densities greater than 1.01 g/cm^3, a value which is often cited[6] as the density of 100% crystalline PE, are predicted for molecular weight values <300 g/mol. If the density of 100% crystalline PE is taken to be 1.00 g/cm^3, a value also commonly cited,[7] then all molecular weight values <800 g/mol must either be excluded from the calculation or assigned the maximum density value.

In the calculations used in this present work, all molecular weights <700 g/mol were assigned density values of 1.006 g/cm^3. It is also plausible that the linear correlation may result in underestimates of the true density at very high molecular weights. However, a simulation of a MWD for an UHMW-PE homopolymer sample (i.e., Gaussian shaped MWD, 2,000 kg/mol M_w and a 4 PDI) yielded a calculated density of 0.932 g/cm^3, which is in line with expected values (i.e., between 0.93 and 0.94 g/cm^3). Therefore we expect the linear range of the calibration curve (Eq. 2) to extend from 0.7 to 1×10^4 kg/mol. This range corresponds to density values of 1.01 to 0.906 g/cm^3, respectively. As shown in Figure 1, the resulting density values predicted from this model as a function of molecular weight compare well to peak molecular weight data given in Table 1.

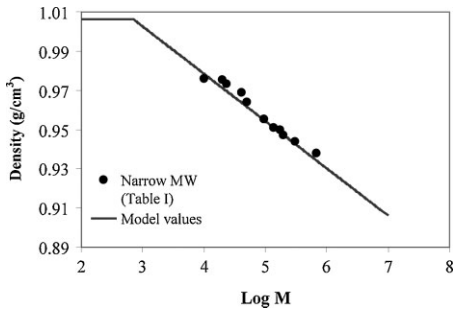

Figure 1.
The calibration curve used to estimate equilibrium densities of polyethylene samples (solid line) and the values for both the measured density and the logarithm of the peak molecular weight of samples listed in Table 1 (solid circles).

Although this method is a simplistic approach, we found that on average, we can predict the densities of polyethylene homopolymers to within $\pm 0.002\,g/cm^3$. This is likely due to the fact that in most polydisperse polyethylene samples, the majority of the sample falls within the linear range of our correlation. A comparison of measured and calculated density values for homopolymers having diverse types of molecular weight distributions is shown in Table 2.

To further account for the added contributions to density suppression by the presence of short chain branching for each MW slice, the difference between the measured bulk density of copolymer and the calculated homopolymer density is divided by the overall SCB level (as measured by SEC-FTIR) and subsequently applied to the SCB level in each MW slice. Typical MWD and SCB data obtained by SEC-FTIR for a bimodal sample are shown in Figure 2. The original observed bulk density of the copolymer (down to $0.852\,g/cm^3$) is obtained through summation of the MW slices as described above. In our present method, we have again simplified the calculations by assuming that all SCB levels will have the same effect on density suppression. However, we recognize that the effectiveness of a particular SCB level to suppress density will vary (i.e., the ability of SCB to disrupt crystallinity decreases as the level of SCB increases). How to address this observation will be the subject of future publications.

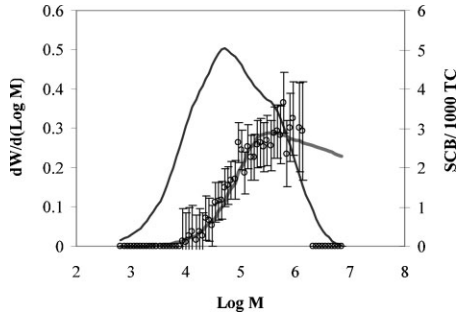

Figure 2.
Typical MW and SCB distribution data acquired using SEC-FTIR. This particular example is for a bimodal type resin where the SCB is located primarily in the high end of the MWD. The solid SCB line in this figure represents the calculated SCBD based on the known weight fraction amounts of SCB in each component.

Probability of tie Molecule Formation

The next step in formulating a primary structure parameter that describes SCG was to factor in the effects of tie molecule formation.[5,7,9–11] The enhanced SCG performance in samples where SCB is primarily on the longest chains in the MWD has long been attributed to the formation of tie molecule by many researchers, including all those referenced in this paper. The theory is that putting more branching on the longer chains forces a portion of the chain into the amorphous region of the polymer while the other parts of the chain are able to incorporate into more than one crystalline lamella and thus increases the probability that they will act as tie molecules, holding the semicrystalline polymer matrix together. In addition to these tie chains which transverse between the crystalline and amorphous portions of the polymer, other structures such a chain entanglements (intertwined loops) located in the amorphous phase can also serve as means by which lamellae can be linked together and

Table 2.
Calculated densities for polyethylene homopolymer samples.

Sample	MWD type	M_w (kg/mol)	PDI	Measured density (g/cm^3)	Calculated density* (g/cm^3)	Absolute Residual
HP-1	monomodal	44	5.7	0.970	0.971	0.001
HP-2	monomodal	81	3.8	0.962	0.962	0.000
HP-3	bimodal	103	7.1	0.965	0.963	0.002
HP-4	monomodal	145	8.7	0.962	0.962	0.000
HP-5	bimodal	250	33.6	0.965	0.962	0.003

*See text.

therefore are also considered to be tie molecules.

In the development of *PSP2*, we chose to capture the level of tie chain content by using the statistical approach originally described by Haung & Brown.[5] This method captures the probability of a molecule with a particular molecular weight (M) and hence chain length, to form a tie molecule by traversing a critical distance L between lamellae as described by Equation 3 below. This of course can be considered the minimum length needed to form a tie molecule and does not address what happens when a chain length is $\gg L$ nor does it consider chain entanglements or branch type.

$$P = \frac{1}{3}\frac{\int_{L}^{\infty} r^2 \exp(-b^2 r^2)dr}{\int_{L}^{\infty} r^2 \exp(-b^2 r^2)dr} \quad (3)$$

where $b^2 = \frac{3}{2\bar{r}^2}$ and $\bar{r}^2 = (Dnl^2)$.

The symbols above have the following meanings:

P = Probability of tie-chain formation
L = Critical distance (nm) = $2l_c + l_a$
D = Chain extension factor in melt = 6.8 for polyethylene
n = Number of links = $M_w/14$ for polyethylene
l = The link length = 0.153 nm for polyethylene

In order to use Equation 3 we must first be able to estimate the lamellar thickness (l_c) and the thickness of the amorphous layer (l_a). From these two values we can then calculate the critical chain end-to-end distance required to form a tie chain (i.e., $2l_c + l_a$). Of the two values, l_c is the dominate variable not only in its coefficient but also in the fact that its value is used to calculate l_a (see below). To calculate these quantities in terms of density per MW slice, we used various literature data on well characterized samples, in particular those reported by Patel[7] and Mirabella.[8] In the Patel studies a series of monodisperse, homogenous ethylene-octene copolymers that spanned a 0.888 to 0.954 g/cm^3 density range were characterized by DSC. In Mirabella's work, both DSC and SAXS data for several metallocene-catalyzed 1-butene copolymers, as well as for selected Zeigler-Natta catalyzed samples were reported. In this latter work the sample densities ranged from 0.865 to 0.965 g/cm^3.

In our work we used the Gibbs-Thompson equation (Eq. 4) to approximate l_c values from each density slice by first developing an empirical calibration curve (Figure 3) that relates density to melting point. This curve is based on T_m and density data from the Patel and Mirabella studies, as well as assigned values for 100% amorphous and crystalline PE samples. Several values for the density of both phases have been reported in the literature. In this study, amorphous phase PE was assigned a 0.852 g/cm^3 density[6] at 20 °C and crystalline PE a density value of 1.01 g/cm^3 at its equilibrium melting temperature (T_m^0). It is obvious from Equation 4 that the assignment of T_m^0 plays a defining role in the final values of both l_c and l_a, and subsequent *PSP2* values. Two values of T_m^0 are typically presented in the literature,[12-15] those close to 141.5 °C and those close to 145.5 °C.

$$\ell_c(nm) = \frac{0.624nm \cdot T_m^0(K)}{T_m^0(K) - T_m(K)} \quad (4)$$

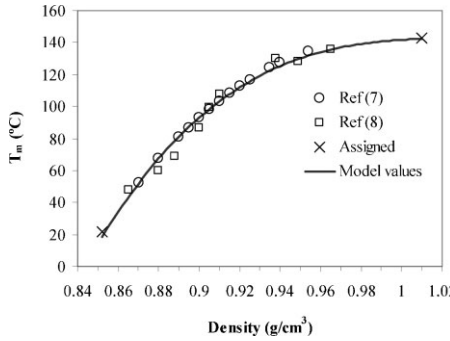

Figure 3.
Empirical calibration curve (solid line) relating density to melting point values compared to respective values reported in the cited references. Assigned values of 20 °C and 142.5 °C were given for density values of 0.852 g/cm^3 and 1.01 g/cm^3, respectively (see text).

For comparison with referenced studies,[7,10,11] a T_m^0 equal to 142.5 °C was assigned to the 1.01 g/cm^3 density slice; the resulting curve of which appears in Figure 3. This plot shows a reasonable relationship between density values and the average melting points (T_m, °C) described by the fitted line. The fitted melting point from the calibration curve for the 1.01 g/cm^3 density was found to be equal to 142.3 °C and is well within the reported[13] uncertainty of the referenced T_m^0 (141.5 ± 1 °C). The calibration curve provides estimates of T_m and ultimately values for l_c via Equation 4 for the respective density at each MW slice. As in the density calculations, a summation of the slice by slice data weighted by the weight fractions (w_i) of the various components that make up the MWD profile yields the respective (l_c) value for the bulk sample.

Although, it is recognized that the Gibbs-Thomson equation has many limitations[7] and that lamellar structure unlikely exists below a 0.90 g/cm^3 density, Equation 4 provides a sound starting point from which a theoretical and general estimate of l_c can be made. For example, the modeled l_c verses density relationship (Figure 4a) was compared to lamellae thicknesses calculated using Equation 4 and the T_m values reported in the Patel and Mirabella studies. As might be expected from the modeled fit of the T_m data as shown in Figure 3, a good agreement exists between all the values calculated using the Gibb-Thompson equation (Figure 4a) as well as reasonable estimations of Mirabella's results using SAXS. The average error between the reported and estimated T_m was ±2 °C.

Also interesting is the observation that when the value of 418.66 K (145.5 °C) is replaced for T_m^0 in Equation 4 and the data recalculated using the appropriate calibration curve for the modeled data, the scatter between all data sets is substantially diminished (particularly at >0.93 g/cm^3) as shown in Figure 4b and a surprisingly good agreement was found between the independent SAXS measurements and all

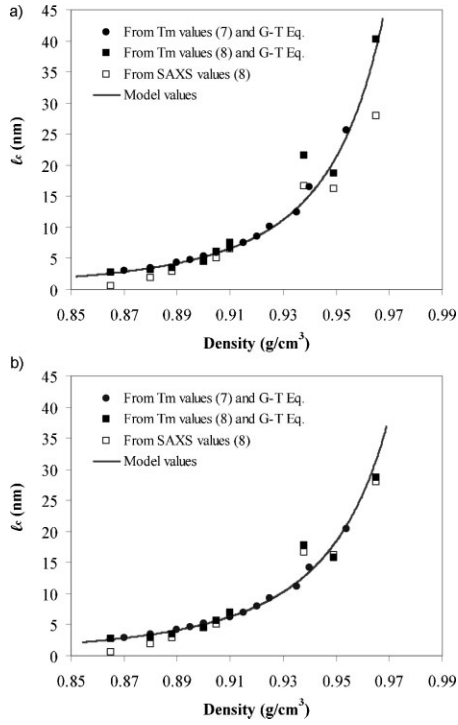

Figure 4.
Estimates lamellar thickness (l_c) plotted against density. Values for l_c were calculated using Equation 4 and a T_m^0 value of 142.3 (a) and 145.5 °C (b).

the Gibb-Thompson generated values (except at densities <0.89 g/cm^3). The implications of using the higher T_m^0 value on calculating *PSP2* will be investigated in future studies.

The thickness of the amorphous layer (l_a) was calculated using the equations 5a and 5b:

$$w_c = \left(\frac{\rho_c}{\rho}\right)\left(\frac{\rho - \rho_a}{\rho_c - \rho_a}\right) \tag{5a}$$

$$\ell_a = \rho_c \ell_c (1 - w_c)/\rho_a w_c \tag{5b}$$

where:

w_c = weight fraction crystallinity
ρ = calculated density of MW slice
ρ_c = density of 100% crystalline sample (assigned 1.006 g/cm^3)
ρ_a = density of amorphous phase (0.852 g/cm^3)

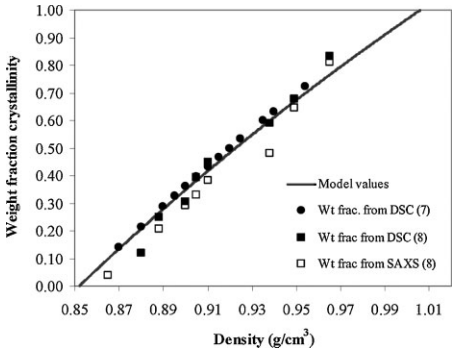

Figure 5.
The values plotted for weight fraction crystallinity (Eq. 5a) as a function of density where the solid line represents modeled values and the points measured data.

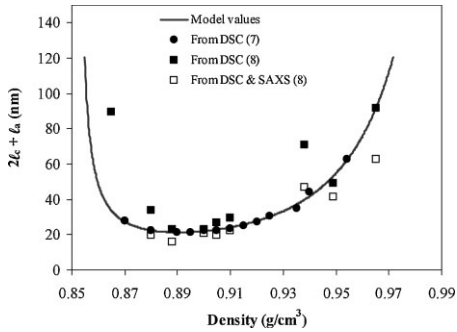

Figure 7.
The values for the quantity $2l_c + l_a$ (i.e., L), as a function of density.

The values for weight fraction crystallinity, l_a, and the quantity $2l_c + l_a$ (i.e., L), as they vary with density, are plotted in Figures 5–7, respectively. Also included in these plots are the corresponding values as measured or recalculated (as in the case of l_a using Eq. 5b) from data reported in the two studies above. Similar to the modeled l_c values, reasonable trends and good approximations to the measured values were found. However, for l_a, a slight upward trend is seen as the density approaches $\sim$0.94 cm^3 before going to zero at 1.01 g/cm3. This trend is eliminated when the 145.5 T_m^0 is used to calculate l_c (data not shown). Another noteworthy point is the correlation between the predicted and reported weight fraction crystallinity which helps validate estimated slice by slice densities used in Equation 4, since the reported data were from direct measurements obtained using two different methods. The above results as a whole suggest that the values predicted from Equation 3, 4 and 5b are adequate for estimating the critical chain end-to-end distance (L) from structural properties.

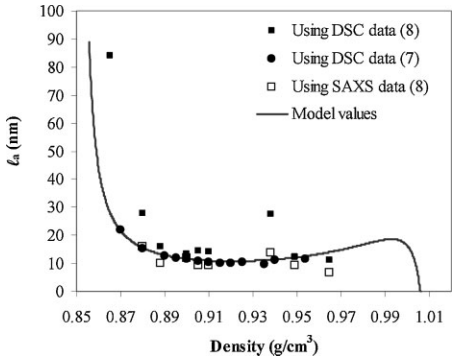

Figure 6.
Values (Eq. 5b) for amorphous phase thickness l_a, as a function of density.

The statistical approach originally described by Haung and Brown gives the probability for a particular molecular length chain, randomly coiled, to span a particular distance L. Since these calculations are for isolated chains, they are ideal for use in our MW slice by slice approach. Excel spreadsheet methods were developed to calculate the slice-by-slice level of tie molecules in a sample using SEC-FTIR data and the probability equation (Equation 3). First, as pointed out by Patel[7] we must recognize that the denominator of the equation for P, the value of the integral from zero to infinity, is given by $\frac{\sqrt{\pi}}{4b^3}$. It is therefore possible to write the expression for P as:

$$P = \frac{1}{3}\frac{\frac{\sqrt{\pi}}{4b^3} - \int_0^L r^2 \exp(-b^2 r^2)dr}{\frac{\sqrt{\pi}}{4b^3}} = \frac{1}{3}\left(1 - \frac{4b^3}{\sqrt{\pi}}\int_0^L r^2 \exp(-b^2 r^2)dr\right) \quad (6)$$

The above integral can easily be set up in an Excel spreadsheet. It is first necessary to enter the molecular weight used and divide by 14 to get the number of links, n. Then the values for $\bar{r}^2$ and b^2 can be calculated using the equations above. A column for values of r needs to be filled out to the largest value of L that is anticipated. A step size of 1 nm for r seemed adequate to give accurate answers. A second column is used to calculate the integrand in the above equation and a third column is used to calculate the cumulative area under that curve using Simpson's rule. The probability of tie-chain formation for any value of r is then obtained by multiplying by the values indicated above. For any critical distance L, the resulting probability can be found by consulting the value of P at $r = L$. Equation 6 produces numerical results ranging from 0 up to 0.333. However we should point out that these probability values are not concentration values in terms of tie molecules per lamellae.

To better understand how the resulting probability value relates to structure, let's consider two ideal polymers, both have M_w values of 100 kg/mol and are essentially monodispersed ($M_w/M_n = 1.001$), Gaussian-shaped MWDs, however, one is assigned a 0.954 g/cm^3 density (no SCB) and the other a 0.90 g/cm^3 density with a flat SCB distribution. At the 100 kg/mol slice of the high density sample's MWD, there is associated a particular density and a corresponding L value of 62 nm estimated as described above. Using Equation 6, a probability value of 0.007 is calculated for this MW slice. Normalizing this value by 0.333 tells us that only 2% of the various random coil chain conformations (via a Gaussian distribution) are able span the corresponding L.

Conversely, for the same MW slice of the low density sample, which has the same chain conformation distribution, the distance L at that slice has now decreased to 22 nm (i.e., smaller l_c since the density of 100 kg/mol slice has decreased). As a result, a probability value of 0.255 is calculated, which in turn tells us that in this sample 77% of the various random coil chain conformations are able to span the corresponding L. These results trend in the right direction for what we would expect for these two types of samples. How well our calculated probability values for tie molecule formation in whole polymer systems compare to those reported in the literature will be left for future discussions.

In formulating the new primary structural parameter, a pragmatic view of the meaning and application of the probability value was taken. It is clear from the above example and other studies[9–11] that the magnitude of the probability value is closely associated with structural properties, despite concerns over particular theoretical underpinnings and limitations of this value. Therefore the value given by Equation 6 was treated essentially as a weighing factor (P_i) for each slice of the MWD and in keeping with the magnitude of *PSP1* values reported in our previous studies,[4] P_i was arbitrarily multiplied x100 and subsequently defined as $PSP2_i$. As in all of our calculations above, this value at each slice was multiplied by the respective weight fraction (w_i) of the MWD profile in order to obtain a value for the bulk polymer. A plot of the calculated (w_i $PSP2_i$) values against log M is shown in Figure 8 for the same bimodal sample depicted in

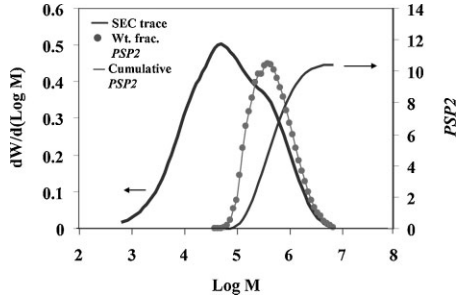

Figure 8.
A plot of the calculated weight fraction *PSP2* (solid circles) and cumulative *PSP2* values (solid line) against log *M* across the MWD is shown for the same bimodal sample depicted in Figure 2. The area underneath the resulting $w_i PSP2_i$ vs. log *M* curve defines *PSP2* for the whole polymer sample. For this particular sample *PSP2* = 10.3.

Figure 2. Also shown in Figure 8 is a plot of the cumulative *PSP2* across the MWD which can also be insightful when attempting understand and predict structure property relationships.

Qualitative Structure Property Relationships

From a qualitative standpoint, if indeed this parameter relates to SCG resistance, we should expect certain directional trends in *PSP2* values that result from specific structural changes. For example, in high molecular weight polymers, longer chains are much more likely to have and maintain entanglements during the crystallization process such that a given chain may be partly in several or even many crystallites. Those portions of the molecules not in the crystallites act as ''tie molecules'' between crystallites. These tie molecules and the amorphous regions in which they are found are believed to be a good part of the reason why higher molecular weight homopolymers are less brittle than low molecular weight varieties. They contribute to the higher impact properties and greater stress crack resistance of high molecular weight polymers. Furthermore, studies of Brown and others[5,16] suggest that a minimum M_w of 18 kg/mol is needed before tie molecules can form. Therefore we should expect an increase in *PSP2* values as the sample's molecule weight increases beyond some critical molecular weight. This is indeed what we find.

In the case of a critical molecular weight, it is observed that MW slices less than ~60,000 g/mol contribute very little to the overall *PSP2* values, as is apparent in the data plotted in Figure 8. A similar finding was reported by Huang & Brown[5] when considering the probability of tie molecule formation for a monodisperse polymer if the long period ($l_c + l_a$) is 27 nm. However, to unequivocally demonstrate the effects of molecular weight on the *PSP2* value is less straightforward due to complex interactions between structural parameters. For example, when *PSP2* values are plotted against molecular weight for monodisperse

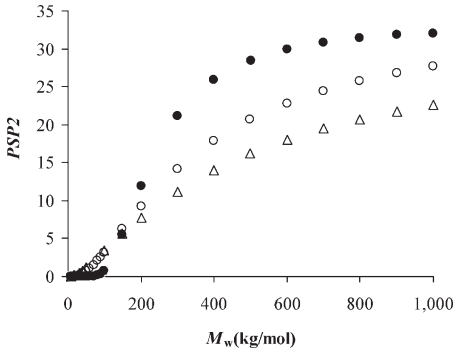

Figure 9.
Effect of increasing M_w and MWD on *PSP2* values calculated for digitally synthesized homopolymers (Gaussian MWD curves) for where $M_w/M_n = 1.01$ (solid circles), $M_w/M_n = 2.0$ (open circles) and $M_w/M_n = 4.0$ (open triangles).

samples (i.e., $M_w/M_n = 1.0000$), the expected increase in the calculated *PSP2* values as *M* increases is obtained (Figure 9).

However, the increase in molecular weight is accompanied by lower sample density (smaller *L* length); which in turn would also result in expectedly higher *PSP2* values. Furthermore, Figure 9 demonstrates the additional complexities that arise when considering samples with polydispersities >1. For a monodisperse sample, the maximum value for *PSP2* (33.3) is reached at ~6,200 kg/mol and at a calculated density of ~0.911 g/cm^3 ($L = 24$ nm). However, it is clear that this is not the case for polydispersed samples. Moreover, because of an increase in the amounts of high molecular weight components in these samples, the *PSP2* values are larger at lower M_w values when compared to the monodisperse samples. To circumvent these difficulties in accessing MW effects on the *PSP2* value, two digital homopolymers structures having different M_w values at the same density were examined. Although density is not an independent variable, by keeping density constant (similar overall *L* values) the influence of M_w can be better conceptualized. Figure 10 and the resulting data given in Table 3, demonstrate the expected increase in *PSP2* values with an increase in M_w.

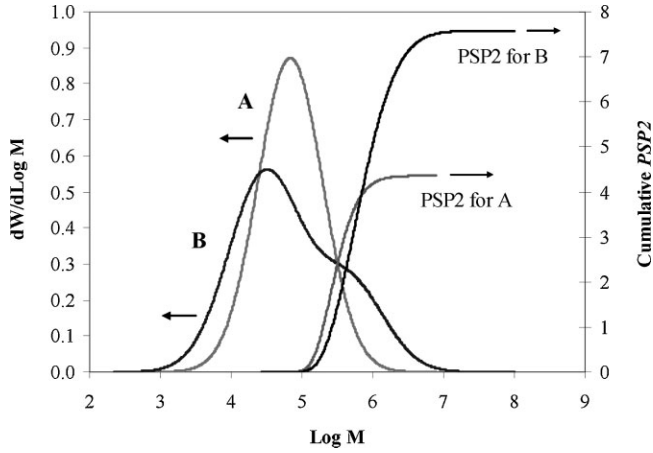

Figure 10.
Cumulative *PSP2* values for two digital homopolymers structures having different M_w values at the same density (also see Table 3).

Another important structural feature that is known to influence SCG resistance is the distribution of SCB along the MWD. It has long been recognized that even for high molecular weight polymers, the impact, and especially the stress crack resistance of the material is improved if the long molecules contain a significant frequency of short chain branches. These tend to increase the number of tie molecules and reduce the size (thickness) of the crystallites and substantially influence the rate of slow crack growth in polyethylene resins.

For example, for many of the pipe resins that meet the ''PE-100'' criteria (i.e., pipe must withstand a hoop stress of 10 MPa for up to 50 years at 20 °C), the distinguishing molecular feature is a high degree of SCB on the longest chains in the molecular weight distribution (MWD). This type of SCB distribution is contrary to that found in PE-80 type resins where higher SCB levels are typically concentrated in the shortest chains of the MWD. Some reasons to why SCB placement on the longest chains enhances SCG performance have been suggested by Krishnaswamy and others.[17]

In Figure 11 a digital blend of two narrow MWD peaks is shown. In Structure C, the representative MWD profile is given for when neither of the two components contains comonomer (i.e., MWD of a homopolymer). In Structures D and E, the SCB was placed in the low and high molecular weight components, respectively. As shown in the calculated properties of

Table 3.
Calculated properties of digital structures given in Figure 10.

Digital structure	M_w (kg/mol)	PDI	Density (g/cm^3)	*PSP2*
A	119	3.1	0.958	4.4
B	307	14.8	0.958	7.8

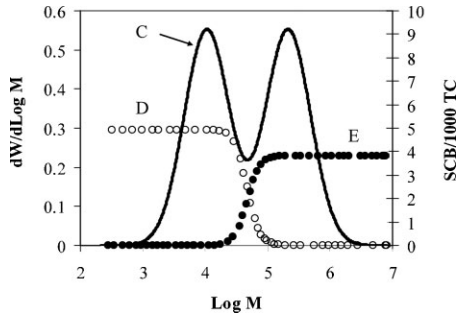

Figure 11.
Molecular weight and SCB distributions for bimodal digital structures where Structure C represents a homopolymer with no SCB and Structures D and E represent the same MWD as C, but with SCB located in the low and high MW end of the MWD, respectively. Table 4 gives the calculated properties for each structure.

Table 4.
Calculated properties of digital structures given in Figure 11.

Digital structure	*M* w (kg/mol)	PDI	SCB/1000 TC*			Density (g/cm^3)	*PSP2*
			LMW component	HMW component	Bimodal blend		
C	157	11	0	0	0	0.962	7.08
D	157	11	4.9	0	2.5	0.950	7.10
E	157	11	0	4.0	2.0	0.950	11.5

*SCB values rounded up to two significant figures.

these structures (Table 4), a dramatic increase in the magnitude of the *PSP2*

value results when SCB is preferentially placed in the high MW end of the MWD of a sample at a specific density. Note that more SCB is needed in Structure D than in E to reach an equivalent density due to the increased amount of higher density material compared to Structure E. However, the *PSP2* values for the homopolymer Structure C and copolymer Structure D are essentially the same within two significant figures. These results show how placement of SCB in the low end of the MWD can affect density, yet does not affect SCG resistance. In this case, the *L* values at MW slices $> 60{,}000$ g/mol are the same for both structures. Krishnaswamy *et. al* [17] have experimentally demonstrated the above structure property relationships by examining the SCG performance of physical blends made from narrowly disperse, polyethylene homopolymer and copolymer components. It is clear that the proposed *PSP2* value is able to qualitatively reflect known structure property relationships.

Quantitative Structure Property Relationships

To test how well *PSP2* values quantitatively predicted slow crack growth resistance, calculated *PSP2* values for four sets of polyethylene resins (Table 5) were compared to short-term test results. The error in the *PSP2* values arising from the ± 0.002 g/cm^3 error in the estimated density propagates as a ± 0.5 in the *PSP2* value. The precision of the *PSP2* value based on multiple SEC-FTIR runs of the same sample (using the measured density for all runs) was found to be ± 0.3.

The first set of samples examined was from data reported by Huang and Brown.[9,10] In these studies Pennsylvania Notch Test (PENT) results conducted at 3 MPa were reported for a series of chromium-catalyzed resins. If reported levels of tie molecules[9] are converted to *PSP2* values and plotted against the

Table 5.
Selected properties for various polyethylene samples.

Sample Set	Number of samples tested	Resin architecture	Nominal M_w range (kg/mol)	Nominal density range (g/cm^3)	Short-term test
1*	6	unimodal CrO_2 resins	126–170	0.938–0.964	PENT @ 3.0 MPa, 80 °C
2	11	unimodal CrO_2 and ZN bimodal resins	193–320	0.947–0.957	PENT @ 2.4 MPa, 80 °C
3	15	unimodal CrO_2 and ZN resins; bimodal ZN resins	150–250	0.935–0.962	SP-NCTL
4	29	unimodal CrO_2, ZN and metallocene resins; bimodal ZN and metallocene resins	119–320	0.910–0.962	Tensile Testing (NDR)

*Reported by Haung & Brown.[9,10]

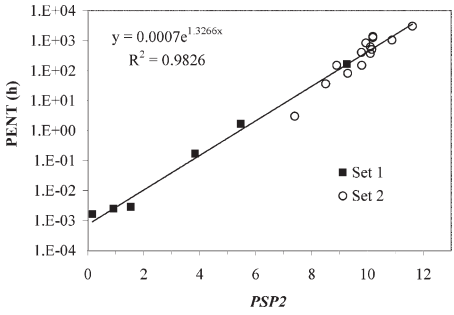

Figure 12.
Correlation between *PSP2* and measured PENT values for resins in set 1 and 2 as described in Table 5.

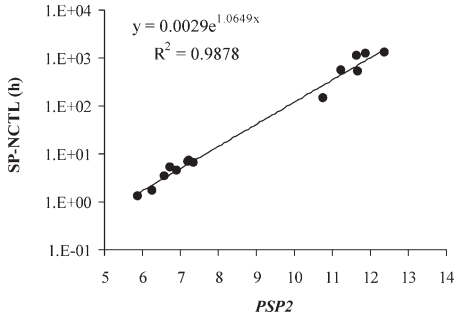

Figure 13.
Correlation found between *PSP2* and SP-NCTL test values for resin set 3.

reported PENT values at 80 °C,[10] we find an evident correlation as shown in Figure 12. From this plot one can see a steady increase in PENT performance as the *PSP2* value increases. SEC-FTIR data were acquired for the remaining three sample sets and the *PSP2* values calculated. These sets are composed of resins with diverse architectures. For resin set 2, we found that a good correlation up to 1000 h also results when *PSP2* values for these samples are plotted against their measured PENT values (PENT studies conducted at 2.4 MPa). In fact, when data from sets 1 and 2 are combined as shown in Figure 12, a very good correlation is observed despite the slight differences in the test conditions.

It is evident from these results that our method as described is able to distinguish the PENT performance based solely on primary structural parameters. However, since the correlation described is based on a log plot of PENT failure times, differentiating a resin's performance becomes problematic as performance approaches 500 h since samples with similar or small changes in *PSP2* values can have vastly different PENT values. For example, for those samples having *PSP2* values equal to 10.2, the respective PENT values ranged from 500 to 1300 h. We should also note that we are currently investigating whether the power law correlation between *PSP2* and PENT values is valid beyond 1000 h test times for all resin architectures. *PSP2* values were also compared to other SCG tests results such as the Single Point Notched Constant Tensile Load test (SP-NCTL) and Natural Draw Ratio (NDR). In Figure 13 a plot of *PSP2* values vs. SP-NCTL results for sample set 3 is given. Once again, a good correlation was found between *PSP2* values and the short term test results for this sample set despite structual differences.

Similarly a correlation was found between NDR results and *PSP2* values (Figure 14) for architecturally different samples as described in sample set 4. This latter sample set extends over the end use application range for polyolefins. Particularly interesting in Figure 14 is the observation that bimodal pipe samples with 0.950 g/cm^3 densities and geomembrane

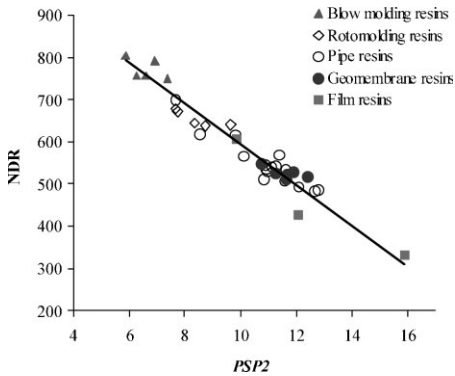

Figure 14.
Correlation (RSQ = 0.94) found between *PSP2* and NDR test values for resin set 4. Error for *PSP2* values estimated to be ±0.5.

samples (~0.935 g/cm^3) have similar NDR values despite the density differences. This fact further demonstrates the effects of SCB placement on SCG resistance and the ability of *PSP2* to capture this structural effect.

Conclusion

In this work primary structures such as molecular weight and short chain branching, as well as their respective distributions, were used to formulate a single parameter (*PSP2*) capable of rapidly estimating the potential slow crack growth resistance of polyethylene resins as determined by short term testing methods. This method is based on experimental data obtained directly from SEC-FTIR, bulk density values, and statistical calculations for tie molecule probabilities as described by Huang & Brown. The statistically acquired probability value was treated essentially as a weighing factor (P_i) for each slice of the MWD. P_i was arbitrarily multiplied x100 and subsequently defined as $PSP2_i$. The summation of (w_i $PSP2_i$) across the MWD profile defines *PSP2* for a particular resin.

The calculations of P_i principally rely on density estimates on a MW slice by slice basis, from which subsequent estimates of melting point and lamella thickness were made in order to obtain the critical chain end-to-end distance required to form a tie chain (i.e., $2l_c + l_a$) as described by Huang & Brown. We found that the effects of primary structure on density and corresponding T_m values can be empirically estimated across the molecular weight distribution to within average values of ± 0.002 g/cm^3 and ± 2 °C, respectively. From these values and known relationships such the Gibbs-Thompson and percent crystallinity equations, values for $2l_c + l_a$ were approximated. The estimated thicknesses for both l_c and l_a appear to be consistent with those reported in the literature when assessed using comparable values for ρ_c, ρ_a and T_m^0. This method assumes a constant effect of SCB levels on density and is limited to average values for SCB, T_m, etc. per MW slice. Moreover, the method does not take into account branch type.

Finally, calculated *PSP2* values for several digitally generated and experimentaly obtained MWD and SCB profiles demonstrated both the qualitative and quantitative use of this single parameter to capture known structural effects on SCG resistance. Most notably is the ability of this parameter to successfully predict the effects of SCB placement on SCG properties. We found that *PSP2* values corresponded well for the slow crack growth (SCG) resistance in all types of polyethylene resins as reflected by power law correlations to PENT values (up to 1000 h) and SP-NCTL results, as well as a linar corelation to NDR tensile testing. Even when the cited limitations for this method are considered, our results demonstrate that *PSP2* values can be used to screen resins for potential SCG performance using resin microstructure. Moreover, since this method is based on structural parameters, its use and further development are expected to help better understand the SCG failure mechanisms in PE resins while improving the cost and effectiveness of product design.

Acknowledgements: The authors would like to acknowledge numerous colleagues at Chevron Phillips Chemical Company for helpful conversations, particularly Drs. Dave Register and Ashish Sukhadia. We also thank Mr. Alan Miller and Mr. Jim French for their technical assistance.

[1] P. J. DesLauriers, D. C. Rohlfing, E. T. Hsieh, *Polymer* **2002**, *43*, 159.
[2] P. J. DesLauriers, *ACS Symposium Series* **2005**, *893*, 210.
[3] Chung C. Tso, P. J. DesLauriers, *Polymer* **2004**, *45*, 2657.
[4] P. J. DesLauriers, Polyolefins 2006 Conference Proceedings, February 28- March 1,Houston, TX, **2006**. Inital concepts of *PSP2* were also indrodued at this conference. Also see P. J. DesLauries and D.C. Rohlfing in *2006 Plastic Pipe XIII Conference Proceedings*.
[5] Y. L. Huang, N. Brown, *Journal of Materials Science* **1988**, *23*, 3648.

[6] K. Jordens, G. L. Wilkes, J. Janzen, D. C. Rohlfing, M. B. Welch, *Polymer* **2000**, *41*, 7175.
[7] R. M. Patel, K. Sehanobish, P. Jain, S. P. Chum, G. W. Knight, *J. Appl. Poly. Sci.* **1996**, *60*, 749.
[8] F. M. Mirabella, A. Bafna, *Journal of Polymer Science, Part B: Polymer Physics* **2002**, *40*, 1637.
[9] Y. L. Huang, N. Brown, *Journal of Polymer Science, Part B: Polymer Physics* **1990**, *28*, 2007.
[10] Y. L. Huang, N. Brown, *Journal of Polymer Science, Part B: Polymer Physics* **1991**, *29*, 129.
[11] R. Seguela, *Journal of Polymer Science, Part B: Polymer Physics* **2005**, *43*, 1729.
[12] B. Wunderlick, G. Czornyj, *Macromolecules* **1977**, *10*, 960.
[13] L. Mandelkern, G. M. Stack, *Macromolecules* **1984**, *17*, 871.
[14] P. J. Flory, A. J. Vrij, *J. Am. Chem. Soc.* **1963**, *85*, 3548.
[15] L. Lu, R. G. Alamo, L. Mandelkern, *Macromolecules* **1994**, *27*, 6571.
[16] X. Lu, N. Ishikawa, N. Brown, *Journal of Polymer Science, Part B: Polymer Physics* **1996**, *34*, 1809.
[17] R. Krishnaswamy, Q. Yang, L. Fernandez-Ballester, J. A. Kornfield, *Macromolecules* **2008**, *41*, 1693.

